journal

J. Am. Ceram. Soc., 80 [5] 1245–55 (1997)

Composite Laminates in Plane Stress: Constitutive Modeling and Stress Redistribution due to Matrix Cracking

Guy M. Genin and John W. Hutchinson*

Harvard University, Cambridge, Massachusetts 02138

Plane-stress constitutive relations for laminate composites undergoing matrix cracking are developed that can be fit to data from uniaxial tests. The constitutive equations are specialized to brittle-matrix composites in the form of crossplies and quasi-isotropic laminates. The effect of nonlinear stress–strain behavior on stress redistribution around holes and notches in laminate plates is illustrated.

I. Introduction

FIBER-REINFORCED brittle-matrix composites are of technological interest as potential lightweight materials for high-temperature environments. Design with brittle-matrix composites is typically based on linear elastic stress analyses, and components made of such composites are usually constructed so as to avoid all cracking at design loads. This approach is unduly conservative for certain classes of fiber-reinforced ceramic-matrix composites that possess appreciable "ductility" associated with matrix cracks that leave the fibers intact. Allowance for some matrix cracking at points of high stress concentration can considerably increase the load-carrying capabilities of some of these materials. In these laminates, the nonlinear stress–strain behavior associated with matrix cracking can redistribute and reduce stresses in regions of high stress concentration, similar to the way that plastic deformation accommodates stress concentration in metals.

An example of a composite that displays some ductility is coated silicon carbide (SiC) fibers embedded in a glass (calcium aluminosilicate, CAS) matrix. When SiC/CAS laminae are stacked in a (0°/90°) crossply configuration and loaded in uniaxial tension, the stress–strain behavior of the laminate is as shown in Fig. 1(A), as reported by Cady[1] and Beyerle *et al.*[2] The material responds linearly to the point at which the matrix material begins to crack, then loses stiffness as an increasing number of matrix cracks form.[2,3] The cracks that are growing in the matrix material deflect into the low-toughness fiber/matrix interfaces, given an appropriate fiber coating, and eventually arrest,[4,5] leaving the fibers intact. When the matrix material becomes saturated with cracks, all the load is taken by the fibers, which deform in a linear elastic fashion until failure. When the fibers do start to fail, they do not necessarily break at the matrix–crack plane; consequently, they continue to provide some load-carrying capacity because of frictional pullout. The data shown in Fig. 1(A) has been taken under nominally load-controlled conditions. If the data had been taken in a controlled-displacement tensile test, a portion of the stress–strain curve with decreasing stress after the peak would be observed.

Figure 1(A) also shows the Cady data[1] for the strain transverse to the loading direction in a uniaxial tensile test that has been conducted parallel to a set of fibers in the SiC/CAS crossply. The material experiences the usual Poisson contraction in the linear range; however, as matrix cracks deflect into the fiber/matrix interfaces and the fibers become increasingly debonded, the transverse strain is largely uncoupled from the uniaxial stress and the strain increments reverse sign. By the point at which the matrix material becomes saturated with cracks, some composites actually experience an expansion in the transverse direction.

Figure 1(B) shows the uniaxial and transverse strains resulting from a controlled-force tensile test that has been conducted at an angle of 45° to the fiber directions in a SiC/CAS crossply. The curves illustrate a different behavior from that exhibited in the previous loading, with extensive straining at nominally constant stress once matrix cracking is underway. The matrix cracks still form perpendicular to the direction of the maximum principal stress; however, now the fibers are not oriented to carry the applied stress nearly as effectively as when the stress acts parallel to one set of fibers. If the matrix were not present, the crossed fibers would simply deform by a "scissoring" mechanism. The uncracked matrix suppresses this mechanism but matrix cracking permits its partial operation. The density of matrix cracks at saturation is generally much higher for the 45° loading than for the 0° loading. This effect may be increased by a porous matrix or strong elastic anisotropy in the fibers. However, the matrix cracking stress and even the elastic modulus for loading at an angle of 45° to the fiber directions may be higher or lower than the corresponding quantities for loading parallel to the fibers, depending on the properties of the constituents of a laminate. Transverse to the loading direction, the response of the SiC/CAS laminate differs significantly from the transverse response that is observed in Fig. 1(A). After the 45° matrix cracking stress is attained, the composite experiences continued negative transverse straining with strains on the order of the strain in the direction of loading. This behavior is readily understood in terms of the scissoring mechanism.

The stress–strain curve for the SiC/CAS crossply subject to a shear stress applied parallel to the fibers is shown in Fig. 1(C). It is quite similar to the curve for uniaxial tension at an angle of 45° to the fibers, with the composite exhibiting comparable ductility.

Brittle-matrix laminates that are suitable for engineering have a tendency to be one of two types. Either they behave as SiC/CAS, with a strain to failure both in tension parallel to the fibers and in shear that exceeds the linear elastic strain for the corresponding failure load by a moderate amount, or they exhibit brittle behavior in tension with a much larger strain to failure in shear, as in carbon–carbon (C/C) composites. An example of the stress–strain behavior of the latter, as reported by Turner *et al.*,[6] Heredia,[7] and Evans,[8] is shown in Fig. 2. Both types of materials are attractive in that they have been observed to redistribute stresses around stress concentrations, sometimes to the point that elastic stress concentrations are completely eliminated before the material fails.[9–13] Such behavior is termed notch insensitivity. In this work, it will be shown that changes in stiffness due to matrix cracking contribute to the notch insensitivity observed in components made of SiC/CAS laminates by forcing the redistribution of stresses away from regions of high

B. N. Cox—contributing editor

Manuscript No. 192578. Received May 30, 1995; approved October 25, 1996.

Supported in part by the ARPA University Research Initiative (Subagreement P.O. KK-3007 with the University of California, Santa Barbara, under ONR Prime Contract No. N00014-92-J1808) and the Division of Applied Sciences, Harvard University.

*Member, American Ceramic Society.

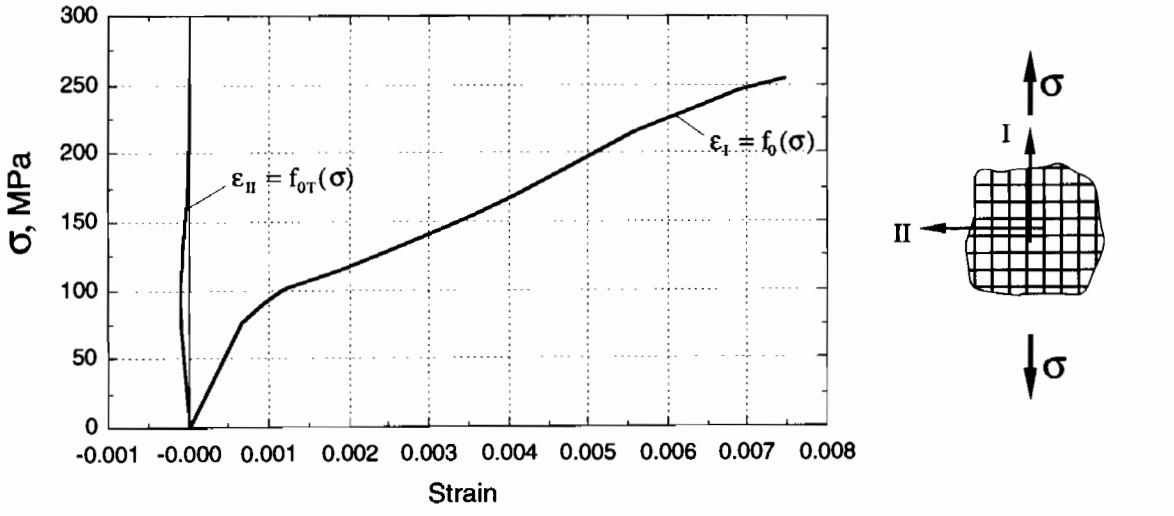

(A)

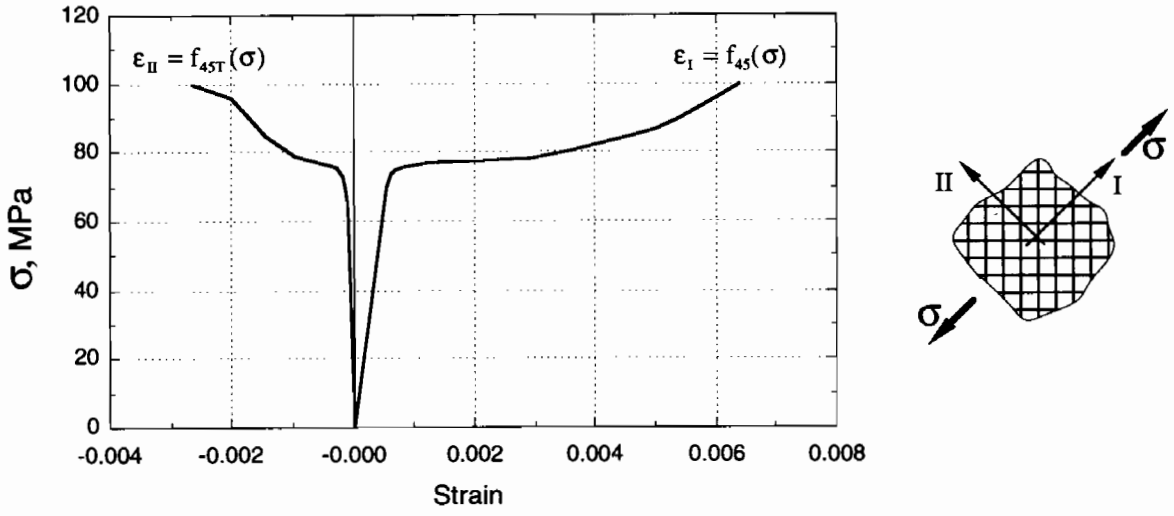

(B)

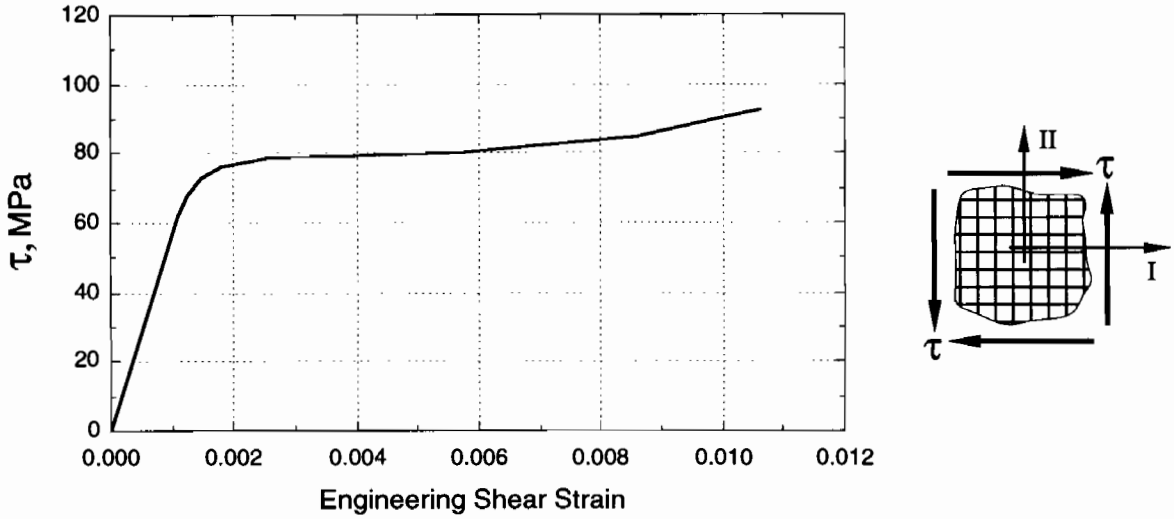

(C)

Fig. 1. Stress–strain behavior of a SiC/CAS crossply in (A) uniaxial tension parallel to the fibers, (B) uniaxial tension at an angle of 45° to the fibers, and (C) pure shear in the fiber axes. Data is from Cady[1] and Beyerle *et al.*[2]

stress concentration. However, in components made of the C/C composite, matrix cracking can actually serve to intensify stress concentrations; the observed notch insensitivity in C/C components is due to phenomena that occur after the carbon fibers begin to fracture.

Stress analysis that accounts for notch insensitivity allows for less-conservative design. The goal of the engineer, and the goal of the present work, is to predict the notch sensitivity of a brittle-matrix laminate in a particular configuration and, thereby, accurately assess the ultimate load and failure mechanism for a component made of these brittle-matrix laminate materials.

Fundamental to such an analysis is a constitutive law that accounts for the inelastic material response of these composites. Although a substantial amount of literature exists for the prediction of the mechanical behavior of laminates of different material systems and stackings based on micromechanical analysis (e.g., Xia and coworkers[14,15] and Dvorak and coworkers[16–18]), the micromechanical approach to design is invariably too complicated to use for generating the constitutive response needed in component stress analysis. Although a few attempts have been made to actually design very simple laminate components from micromechanical analyses for metal-matrix and polymer-matrix composites (e.g., Kennedy and Wang[19] and Dvorak *et al.*[20]), most efforts to develop computational methods of stress analysis to aid in the design of components of brittle-matrix laminates have led to two categories of constitutive relations: continuum damage laws and phenomenological stress–strain laws similar to those for elastic–plastic solids.

Continuum damage mechanics attempt to curve fit experimental data with a set of damage parameters that are considered to be internal variables that evolve with the loading history. Various schemes for modeling the state of degradation of either a lamina or a laminate have included scalar variables,[21–26] damage vectors,[27] and even damage tensors (e.g., Talreja[28] and Allen *et al.*[29]). The approach adopted in the present paper is the phenomenological approach. The focus is on behavior under proportional plane stressing, and the development of the constitutive law parallels that of the deformation theory of plasticity. This entails using data from stress–strain tests and, ignoring details of the internal mechanisms that produce this behavior, creating a scheme that reproduces the input tests and estimates the mechanical behavior for all other multiaxial loadings.

Several phenomenological constitutive models exist in the literature, each of which treats either individual laminae or entire laminates as plane-stress continua and has been designed to model only proportional loading. Petit and Waddoups[30] proposed an incrementally linear orthotropic model, in which the incremental shear and tensile moduli at each point within each lamina are updated to equal the tangent moduli of the stress–strain curves corresponding to the tensile and shear stresses at the beginning of a loading increment. Although their model completely neglects the behavior of the material transverse to the loading direction and, thus, is not applicable to multiaxial stress states, Petit and Waddoups[30] did successfully predict tensile stress–strain curves for uniaxial loadings in different orientations on applying their scheme to laminate composites of different lay-ups, with the laminae constrained by the condition that points in neighboring layers must move together.

Hahn and Tsai,[31] focusing on materials such as the C/C composite, whose behavior is shown in Fig. 2, modeled the behavior of a lamina by combining linear elasticity for the normal components of stress and strain with a nonlinear elastic curve-fit of the shear behavior. Hahn[32] later specialized this model to the case of a 0/90 laminate. Surrel and Vautrin[33] proposed a curve-fit of the nonlinear behavior for loading perpendicular to the fibers in a lamina, in addition to a curve-fit of the nonlinear shear behavior, and then also successfully reproduced off-axis uniaxial test results in a unidirectional laminate. These simple constitutive models are limited in that they are incapable of modeling inelastic behavior that occurs for loading in the fiber axes, such as that observed for the SiC/CAS composite in Fig. 1, and also fail to reproduce the often-reported observation that the maximum inelastic strain in a brittle-matrix laminate occurs in the direction of the largest principal stress. Nevertheless, several authors (e.g., Chang *et al.*[34]) have analyzed multidirectional laminate composites by applying a single lamina constitutive law, similar to that of Hahn and Tsai,[31] to each of the individual laminae of a composite in the manner of Petit and Waddoups[30] and have obtained reasonable qualitative results. Other authors[35,36] used the linear elastic properties of a 0/90 laminate combined with a nonlinear elastic curve-fit of shear behavior in a manner similar to that of Hahn.[32]

The current work presents a plane-stress constitutive model for proportional loading of (0/90) laminate composites that is based on three uniaxial measurements. The formulation also applies to laminates of a (0/±45/90) configuration. The model accurately predicts all additional sets of data that are available for the two material systems introduced above. The model is then used in component-stress analysis and accurately replicates experimental observations and measurements.

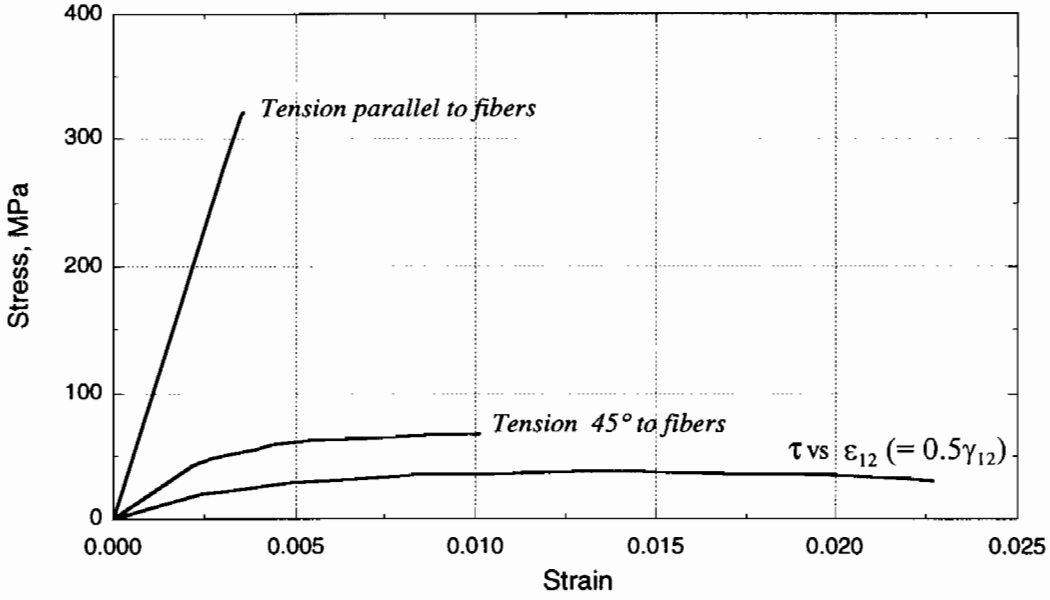

Fig. 2. Stress–strain curves for a C/C crossply (from Turner *et al.*,[6] Heredia,[7] and Evans[8]).

II. Constitutive Model

This section develops a plane-stress constitutive model for symmetrically stacked brittle-matrix laminates. In the first part, the model is developed for "specially orthotropic" laminates, i.e., laminates that possess cubic in-plane symmetry. The most-common examples of these are laminates stacked with a (0/90) configuration and laminates stacked with a (0/±45/90) configuration in which the number of individual plies with a ±45° orientation differs from the number of plies with 0° and 90° orientations. Although the formulation is valid for both systems, attention is focused on the (0/90) configuration.

In the second part, the model is developed for laminates that possess in-plane isotropy. Two common configurations of laminae that produce "quasi-isotropic" laminates are the (0/±60) and (0/±45/90) configurations, the latter only when equal numbers of laminae are oriented in each of the four directions. The constitutive equations for quasi-isotropic laminates are shown to be a special case of the constitutive equations for the crossply laminates.

(1) Crossply Laminates

The most-reliable data on which to base a plane-stress constitutive model are uniaxial stress–strain tests. Let the results of a stress–strain test parallel to the fibers in a crossply composite be denoted by $\varepsilon_I = f_0(\sigma_I)$ for strain parallel to the fibers, in terms of applied stress, and $\varepsilon_{II} = f_{0T}(\sigma_I)$ for strain transverse to the loading direction, in terms of applied stress, as depicted in Fig. 1(A). The following is proposed for proportional multiaxial loading when the principal axes of stress and strain are aligned with the fibers:

$$\varepsilon_I = f_0(\sigma_I) + f_{0T}(\sigma_{II}) \tag{1a}$$

and

$$\varepsilon_{II} = f_0(\sigma_{II}) + f_{0T}(\sigma_I) \tag{1b}$$

This assumes that no interaction exists between these two principal stress components, which is justified on the grounds that matrix cracking perpendicular to one stressing direction decouples the straining in the other direction.

The axes at an angle of 45° to the fiber axes also are symmetry axes. For loading in which the principal axes of stress are aligned at an angle of 45° from the fibers in a crossply, the strains share the same principal axes and are considered here to be given by relations similar to those in Eqs. (1):

$$\varepsilon_I = f_{45}(\sigma_I) + f_{45T}(\sigma_{II}) \tag{2a}$$

and

$$\varepsilon_{II} = f_{45}(\sigma_{II}) + f_{45T}(\sigma_I) \tag{2b}$$

In these equations, $f_{45}(\sigma_I)$ represents strain in the loading direction for a uniaxial tension test conducted at an angle of 45° to the fiber directions, and $f_{45T}(\sigma_I)$ represents strain transverse to the loading direction for this test, as shown in Fig. 1(B).

An important connection follows from the requirement that, for equibiaxial loading with $\sigma_I = \sigma_{II} = \sigma$, the orientation of the principal axes is indeterminate and the strains from Eqs. (1) must match the strains from Eqs. (2). Consequently, $f_{45T}(\sigma)$ may be written in terms of the other three functions as

$$f_{45T}(\sigma) = f_0(\sigma) + f_{0T}(\sigma) - f_{45}(\sigma) \tag{3}$$

In principle, experimental stress–strain data for any three of the four functions appearing in Eqs. (1) and (2) could be chosen, with the fourth given by Eq. (3). In this work, data for the three functions on the right-hand side of Eq. (3) will be input into the model, whereas $f_{45T}(\sigma)$ follows from Eq. (3).

From this point, the formulation continues as a recipe for the stresses in terms of the strains. This is necessary because, for materials of the type being considered, stress component ranges vary significantly for various multiaxial states, whereas strain components are much less restricted. We define $\Sigma_0(\varepsilon_I,\varepsilon_{II})$ as the inverse of Eqs. (1), such that

$$\sigma_I = \Sigma_0(\varepsilon_I,\varepsilon_{II}) \tag{4a}$$

and

$$\sigma_{II} = \Sigma_0(\varepsilon_{II},\varepsilon_I) \tag{4b}$$

The reduction in stresses due to matrix cracking at prescribed ε_I and ε_{II}, when the principal loading axes coincide with the fiber directions, is the difference between the stresses that would result if no cracking occurred and Σ_0. The "stress deficits" for loading in the fiber axes are defined as

$$\Delta\sigma_I^0 = \frac{E_0}{(1-\nu_0^2)}(\varepsilon_I + \nu_0\varepsilon_{II}) - \Sigma_0(\varepsilon_I,\varepsilon_{II}) \tag{5a}$$

and

$$\Delta\sigma_{II}^0 = \frac{E_0}{(1-\nu_0^2)}(\varepsilon_{II} + \nu_0\varepsilon_I) - \Sigma_0(\varepsilon_{II},\varepsilon_I) \tag{5b}$$

where E_0 and ν_0 are, respectively, the elastic modulus and Poisson's ratio for uniaxial loading parallel to the fibers.

Similarly, for the case when the principal axes of loading lie at an angle of 45° to the fiber directions, denote the inverse of Eq. (2) as $\sigma_I = \Sigma_{45}(\varepsilon_I,\varepsilon_{II})$ and $\sigma_{II} = \Sigma_{45}(\varepsilon_{II},\varepsilon_I)$ and let the stress deficits due to matrix cracking be given by

$$\Delta\sigma_I^{45} = \frac{E_{45}}{(1-\nu_{45}^2)}(\varepsilon_I + \nu_{45}\varepsilon_{II}) - \Sigma_{45}(\varepsilon_I,\varepsilon_{II}) \tag{6a}$$

and

$$\Delta\sigma_{II}^{45} = \frac{E_{45}}{(1-\nu_{45}^2)}(\varepsilon_{II} + \nu_{45}\varepsilon_I) - \Sigma_{45}(\varepsilon_{II},\varepsilon_I) \tag{6b}$$

Here, E_{45} is the elastic modulus for uniaxial loading in the axes at an angle of 45° to the fiber directions; ν_{45}, which is the Poisson's ratio in these axes, can be expressed in terms of E_0, ν_0, and E_{45}, using Eq. (3), as

$$\nu_{45} = 1 - \frac{E_{45}}{E_0}(1-\nu_0) \tag{7}$$

Now consider principal strains $(\varepsilon_I,\varepsilon_{II})$ in principal axes oriented at an arbitrary angle θ from the fiber directions. The principal axes of stress deficits due to matrix cracking are considered to coincide with the principal strain axes. The stress deficits in these axes are assumed to be given by interpolation between the stress deficits in the 0° and 45° orientations, according to

$$\Delta\sigma_I = \Delta\sigma_I^0\cos^2 2\theta + \Delta\sigma_I^{45}\sin^2 2\theta \tag{8a}$$

and

$$\Delta\sigma_{II} = \Delta\sigma_{II}^0\cos^2 2\theta + \Delta\sigma_{II}^{45}\sin^2 2\theta \tag{8b}$$

where the stress deficits $\Delta\sigma_I^0$, $\Delta\sigma_{II}^0$, $\Delta\sigma_I^{45}$, and $\Delta\sigma_{II}^{45}$ are given in terms of $(\varepsilon_I,\varepsilon_{II})$ by Eqs. (5) and (6). On rotating back to the fiber axes, one obtains the plane-stress relation for stresses associated with proportional straining to $(\varepsilon_1,\varepsilon_2,\gamma_{12} = 2\varepsilon_{12})$:

$$\sigma_1 = \frac{E_0}{(1-\nu_0^2)}(\varepsilon_1 + \nu_0\varepsilon_2) - \Delta\sigma_I\cos^2\theta - \Delta\sigma_{II}\sin^2\theta \tag{9a}$$

$$\sigma_2 = \frac{E_0}{(1-\nu_0^2)}(\varepsilon_2 + \nu_0\varepsilon_1) - \Delta\sigma_I\sin^2\theta - \Delta\sigma_{II}\cos^2\theta \tag{9b}$$

and

$$\tau = \frac{E_{45}}{2(1+\nu_{45})}\gamma_{12} - (\Delta\sigma_I - \Delta\sigma_{II})\sin\theta\cos\theta \tag{9c}$$

Of the five possible sets of data that could be used as a foundation for the constitutive relations, only three are used. The fact that the constitutive behavior can be modeled with

only three of these five tests is a requirement in the elastic range; beyond the elastic range, this is an assumption that must follow from Eqs. (1) and (2). The validity of this assumption is assessed by evaluating the predictions of the model against the two neglected uniaxial tests: the shear strain, in terms of shear stress, and the transverse strain, in terms of stress applied at an angle of 45° to the fibers. For both of these tests, exact expressions for strains, in terms of stresses, follow from Eqs. (1) and (2). The expression for the transverse strain, in terms of stress applied at an angle of 45°, has been derived above and is given in Eq. (3).

For an applied shear stress, the strains are readily obtained by considering the principal stress state, which occurs in the axes of symmetry at an angle of 45° to the fibers, then rotating back to the fiber axes. In the principal axes, the strain state is given by

$$\varepsilon_{\mathrm{I}} = f_{45}(\tau) + f_{45\mathrm{T}}(-\tau) \tag{10a}$$

and

$$\varepsilon_{\mathrm{II}} = f_{45}(-\tau) + f_{45\mathrm{T}}(\tau) \tag{10b}$$

where, again, $f_{45\mathrm{T}}(\sigma)$ is given by Eq. (3).

Rotating back into the fiber axes, the following expressions are found for the strains that result from the application of a shear stress:

$$\gamma_{12} = 2\varepsilon_{12} = f_{45}(\tau) - f_{45}(-\tau) - f_{45\mathrm{T}}(\tau) + f_{45\mathrm{T}}(-\tau) \tag{11a}$$

and

$$\varepsilon_{11} = \varepsilon_{22} = \frac{1}{2}(f_{45}(\tau) + f_{45}(-\tau) + f_{45\mathrm{T}}(\tau) + f_{45\mathrm{T}}(-\tau)) \tag{11b}$$

Before matrix cracking occurs, $f_{45}(-\tau) = -f_{45}(\tau)$ and $f_{45\mathrm{T}}(-\tau) = -f_{45\mathrm{T}}(\tau)$; therefore, $\varepsilon_{11} = \varepsilon_{22} = 0$. However, once the matrix begins to crack, the model predicts that a specimen loaded in pure shear will expand.

Predictions for the two sets of data that are not included as input into the model are plotted against the experimental data of Cady[1] for the SiC/CAS composite in Fig. 3. The predictions are obtained from the above expressions by matching f_0, f_{45}, and $f_{0\mathrm{T}}$ to the uniaxial experimental data of Cady[1] for positive values of σ and by continuing the linear dependence on σ when σ is negative. The slight discrepancy between theory and experiment in the elastic range is due to experimental error; the measured elastic constants are not quite consistent with each other. Figure 3 shows excellent correlation between the experimental and theoretical curves.

(2) Quasi-Isotropic Laminates

The above approach is applicable to symmetric laminates of any stacking. A case of particular interest is the case of composites with isotropic in-plane behavior, which requires only two input equations. Two examples of such composites, to within a reasonable approximation, are composites with lay-ups of $(0°,\pm 60°)$ and $(0°,\pm 45°,90°)$, which are usually referred to as being quasi-isotropic. As above in Eqs. (1) and (2), the formulation begins with the following proposal for strains in terms of stresses in any set of principal loading axes:

$$\varepsilon_{\mathrm{I}} = f(\sigma_{\mathrm{I}}) + f_{\mathrm{T}}(\sigma_{\mathrm{II}}) \tag{12a}$$

and

$$\varepsilon_{\mathrm{II}} = f(\sigma_{\mathrm{II}}) + f_{\mathrm{T}}(\sigma_{\mathrm{I}}) \tag{12b}$$

where $f(\sigma)$ and $f_{\mathrm{T}}(\sigma)$ are, respectively, the data for axial and transverse strains, in terms of stress, for any in-plane uniaxial tensile loading.

As before, let $\Sigma(\varepsilon_{\mathrm{I}},\varepsilon_{\mathrm{II}})$ represent the solution of Eqs. (12) for σ_{I}, in terms of the principal strains, and $\Sigma(\varepsilon_{\mathrm{II}},\varepsilon_{\mathrm{I}})$ represent the solution for σ_{II}; the strains resulting from any applied loading will produce the principal stresses $\Sigma(\varepsilon_{\mathrm{I}},\varepsilon_{\mathrm{II}})$ and $\Sigma(\varepsilon_{\mathrm{II}},\varepsilon_{\mathrm{I}})$. Define θ as the angle from the x_1–x_2 axes to the principal axes. Transforming the stress tensor back into the x_1–x_2 axes yields the following relations for arbitrary plane-stress loading:

$$\sigma_1 = \Sigma(\varepsilon_{\mathrm{I}},\varepsilon_{\mathrm{II}})\cos^2\theta + \Sigma(\varepsilon_{\mathrm{II}},\varepsilon_{\mathrm{I}})\sin^2\theta \tag{13a}$$

$$\sigma_2 = \Sigma(\varepsilon_{\mathrm{II}},\varepsilon_{\mathrm{I}})\cos^2\theta + \Sigma(\varepsilon_{\mathrm{I}},\varepsilon_{\mathrm{II}})\sin^2\theta \tag{13b}$$

and

$$\tau = (\Sigma(\varepsilon_{\mathrm{I}},\varepsilon_{\mathrm{II}}) - \Sigma(\varepsilon_{\mathrm{II}},\varepsilon_{\mathrm{I}}))\sin\theta\cos\theta \tag{13c}$$

Equations (13) also follow directly from the crossply model. Noting that, for an isotropic composite, $f_0(\sigma) = f_{45}(\sigma) \equiv f(\sigma)$ and $f_{0\mathrm{T}}(\sigma) = f_{45\mathrm{T}}(\sigma) \equiv f_{\mathrm{T}}(\sigma)$, Eqs. (1) and (2) match Eqs. (12). Still defining $\Sigma(\varepsilon_{\mathrm{I}},\varepsilon_{\mathrm{II}})$ as the inverse of Eqs. (1) and (2), the stress deficits in the principal axes may be written as

$$\Delta\sigma_{\mathrm{I}} = \frac{E}{(1-\nu^2)}(\varepsilon_{\mathrm{I}} + \nu\varepsilon_{\mathrm{II}}) - \Sigma(\varepsilon_{\mathrm{I}},\varepsilon_{\mathrm{II}}) \tag{14a}$$

and

$$\Delta\sigma_{\mathrm{II}} = \frac{E}{(1-\nu^2)}(\varepsilon_{\mathrm{II}} + \nu\varepsilon_{\mathrm{I}}) - \Sigma(\varepsilon_{\mathrm{II}},\varepsilon_{\mathrm{I}}) \tag{14b}$$

With these stress deficits being identical in the 0° and 45° axes, Eqs. (8) become trivial. Then, when Eqs. (14) are substituted into Eqs. (9), the linear elastic parts of the two sets of equations cancel, and the quasi-isotropic model of Eqs. (13) is recovered.

III. Applications of Model to Stress Redistribution at Holes and Notches

Two boundary-value problems are now solved using the constitutive model, in conjunction with the finite-element method. Both illustrate how the model can be used to predict stress redistribution and the failure mechanism for composite plates containing holes and notches. Two types of material behavior are considered. The solutions generated for plates with edge-notches are compared with experimentally measured strains for this geometry. Because the constitutive equations proposed above are only intended to be valid to the point at which the first fibers begin to break, the calculations can be expected to retain accuracy only when the strains in the fibers are less than the fiber failure strain. Loads at which fibers are expected to begin to fail will be noted in the sequel.

The results show that matrix cracking accounts for a very large portion of the experimentally observed notch insensitivity that is observed in laminates such as the SiC/CAS composite in Fig. 1. However, the results also show that matrix cracking alone is insufficient to reduce stress concentrations in laminates such as the C/C composite in Fig. 2.

(1) Hole in a Plate

A plate of a crossply brittle-matrix laminate containing a circular hole of radius R is loaded with an applied displacement δ parallel to the fibers, as shown in the insets in Figs. 4(A) and (B). The SiC/CAS composite in Fig. 1 and the C/C composite in Fig. 2 are each considered. The behavior of each crossply is compared to that of the corresponding isotropic composite, whose tensile behavior in any direction is matched to the 0° tensile curve.

The nonlinear problems were solved by the finite-element method. An in-house constitutive subroutine was developed and incorporated into a commercial finite-element program (ABAQUS). The constitutive subroutine is designed such that the stress–strain data that are identified in the above section, together with the fiber orientations, are the only inputs. Although the subroutine is completely capable of incorporating nonlinear compressive behavior into the analyses, all materials considered were assumed to behave linearly in compression to highlight the effects of the inelastic tensile strains due to matrix cracking. Outside the linear elastic range in tension, iteration is required at each load step to obtain the stresses in terms of the

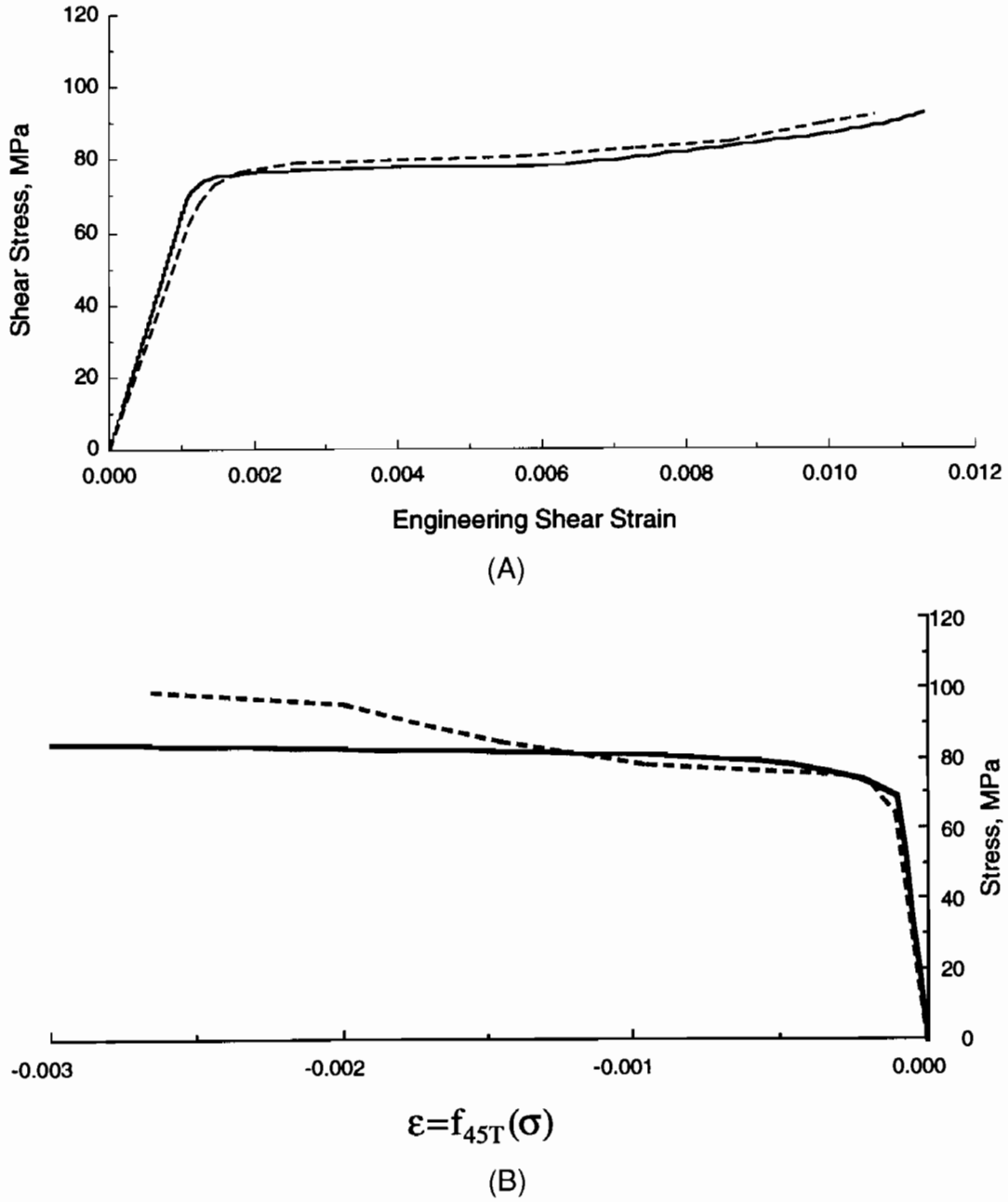

Fig. 3. Predictions for the response of the SiC/CAS crossply composite, compared to data from Cady[1] for (A) shear in the fiber axes and (B) strain transverse to a load applied at an angle of 45° to the fiber axes ((– – –) experiment and (—) prediction).

strains. Eight-noded quadratic elements have been selected for the analyses. Mesh studies have been conducted to ensure accuracy of the computed quantities.

Figures 4(A) and (B) show how the maximum stress concentration in the plate varies as the applied load increases. The point of maximum stress lies on the hole boundary at $(0,\pm R)$. In Figs. 4(A) and (B), this stress is normalized by the linear elastic stress concentration at $(0,\pm R)$. For the SiC/CAS crossply (which is isotropic in the elastic range) and the isotropic composites, this initial stress concentration, defined as the maximum stress divided by the mean stress across the ligament, is 2.5; for the C/C crossply, which is extremely anisotropic in the linear range, the initial stress concentration is 3.85. Solutions for these stress concentrations for the case of an infinite plate can be found in the literature by Green and Zerna.[37]

The C/C composite is significantly weaker in tension at an angle of 45° to the fibers than it is in the fiber axes; consequently, matrix cracking is most pronounced on the boundary of the hole, just behind the point $(0,\pm R)$, as illustrated in Fig. 4(A). As shear cracks develop in a fairly narrow band, leaving the majority of the material that is above the hole and over the ligament uncracked and linear elastic, the stress concentration at the hole increases as a result of the reduction in the tangential shear stiffness of the material directly behind the edge of the hole. Matrix cracking increases the overall compliance of the specimen; that is, it reduces the force increment required to further displace the upper boundary of the material above the hole. However, the cracking also causes the material to lose the shear stiffness necessary to distribute this force over the ligament and away from the hole boundary, and the end result is an increase in the stress concentration.

Despite the large shear concentrations, the C/C crossply will most likely begin to fail in tension, starting at the point $(0,R)$. Failure will occur in this fashion because the shear strain at every point throughout the domain is less than the shear strain that would cause failure in a shear test when the normal strain that would cause failure in a uniaxial tension test is exceeded.

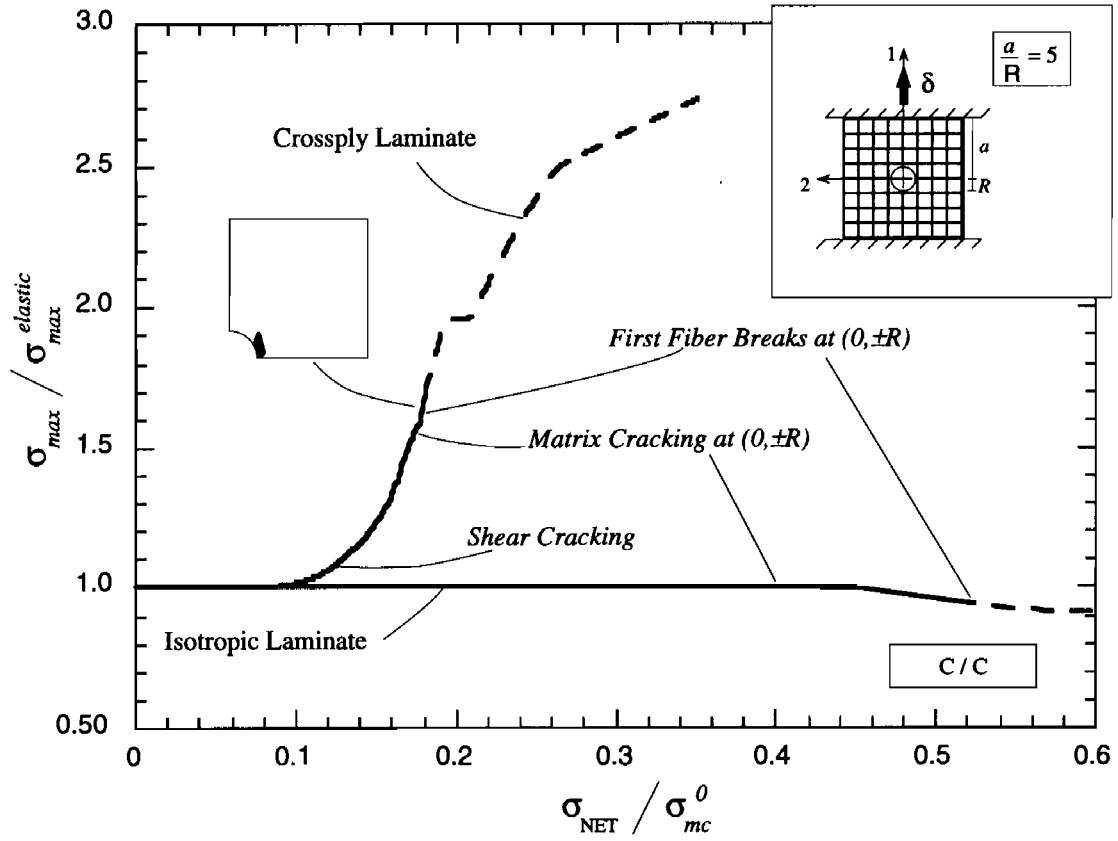

(A)

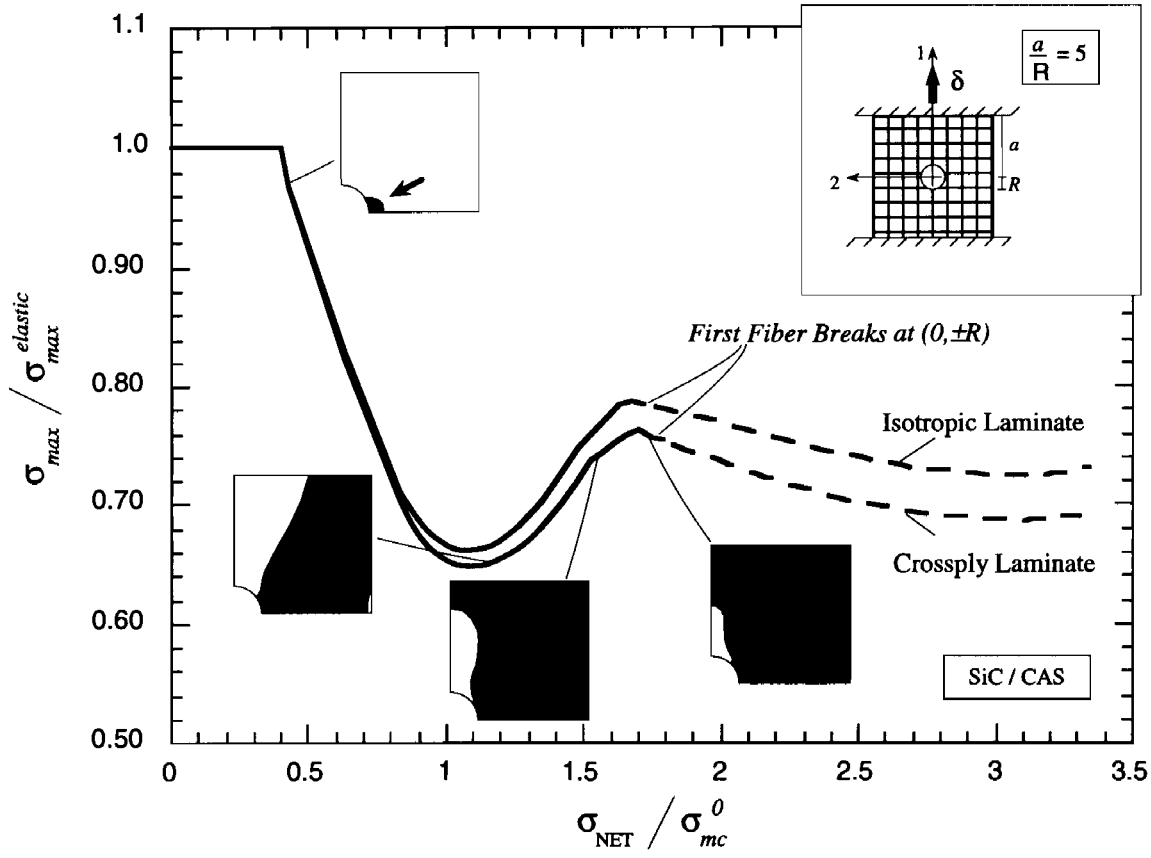

(B)

Fig. 4. Variation of stress concentration factor (SCF), $\sigma(0,\pm R)/\sigma_{NET}$, with respect to the net section stress, defined as the mean stress across the ligament for (A) C/C and (B) SiC/CAS composites. SCFs are normalized by the elastic SCFs (3.85 for the C/C crossply; 2.5 for the SiC/CAS crossply, which is isotropic in the elastic range). Shaded areas of the figures indicate the extent of matrix cracking in the specimens at specific loads.

The isotropic version of the C/C composite cracks first at the point $(0,R)$. After a slight decrease in the stress concentration that is due to a small reduction in axial stiffness that occurs before the failure strain of the fibers is attained (cf. Fig. 2), the stress attains the value that would cause fiber failure in a uniaxial loading of the C/C crossply. The hypothetical isotropic version of this laminate can withstand a higher load than the crossply before fiber failure because of the substantially lower stress concentration. However, this does not necessarily imply that a quasi-isotropic composite is superior for this loading; a $(0/\pm 60)$ laminate, for example, would have a somewhat lower ultimate stress than the crossply, which would have to be considered.

To accurately continue either of the above analyses beyond the point at which the first fiber fails, an analysis of the bridged, propagating crack would need to be performed. Nevertheless, to evaluate the impact of the decrease in axial stiffness on the stress concentration, the analysis is continued by extrapolating the input stress–strain data to the constitutive law as if no fiber failure had occurred. The dashed lines in Figs. 4(A) and (B) indicate that the small decrease in the stiffness of the material at the hole boundary that occurs just prior to the expected first

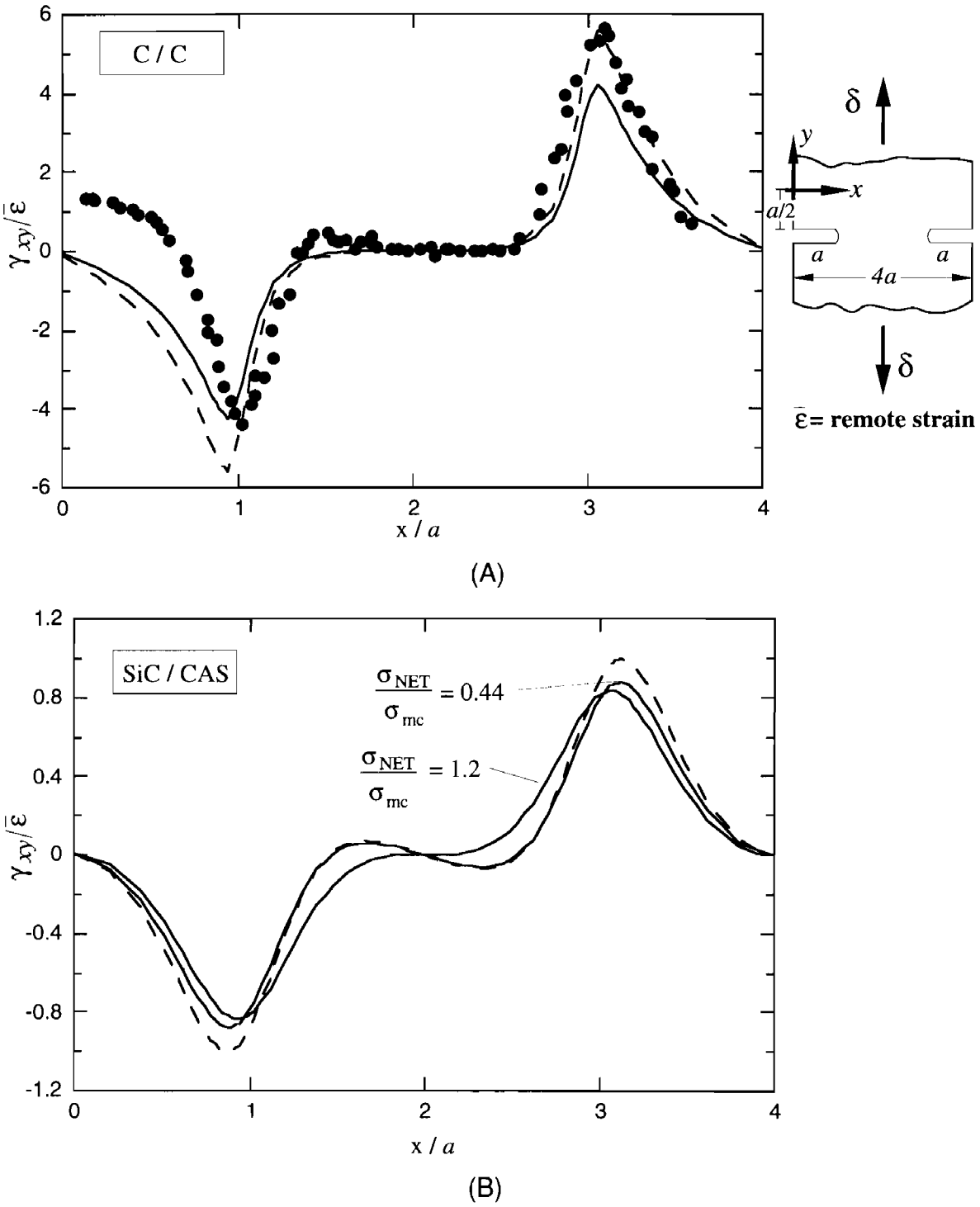

Fig. 5. Engineering shear strains ($\gamma = 2\varepsilon_{12}$) along a line one-half notch length (i.e., $0.5a$) above the notches in double-edge-notched specimens constructed of (A) C/C ((●) experiment (various loads), (---) elastic, and (—) $\sigma_{NET}/\sigma_{mc} = 0.1$) and (B) SiC/CAS ((– – –) elastic). Experimental data plotted in Fig. 5(A) is from Evans.[8]

fiber failures, albeit an effective means of stress redistribution, is insufficient to reduce the stress concentration to beneath the linear elastic value for the C/C crossply.

The response of the SiC/CAS composite, whose matrix cracking strength at an angle of 45° to the fiber axes is comparable to its matrix cracking strength in the fiber axes (cf. Fig. 1), is shown in Fig. 4(B). For this material, matrix cracking first occurs on the hole boundary at the point $(0,R)$, and the stress concentration decreases steadily until matrix cracking extends from the hole boundary to the corners of the plate. The rate of increase of the stress concentration slows when the cracked region extends across the entire top of the plate, and the stress concentration then decreases slightly as cracks develop above the hole.

The curve corresponding to the isotropic version of the SiC/CAS laminate in Fig. 4(B) closely follows that of the crossply. Two conclusions can be drawn from this result. First, the tangent modulus of the material at the hole boundary is the most important parameter in the problem; any mechanism that can reduce the tangent modulus or extend the matrix cracking region of the uniaxial stress strain curve will contribute strongly to stress redistribution. Second, for crossplies that are isotropic in the linear range, the computationally more efficient isotropic material model provides an excellent approximation to the material behavior, assuming that the stress of interest in the body acts parallel to the fiber axes.

In all the cases considered, stressing is approximately proportional throughout the entire loading history (i.e., the relative magnitudes of the stress components at each point are approximately independent of loading). This is essential if the nonlinear constitutive model introduced in this paper is to replicate material behavior accurately.

This simple example clearly shows the utility of the plane-stress analysis incorporating the nonlinear behavior of the material. In both cases, elastic stress concentrations are altered by the mechanism of matrix cracking, and the actual load at which failure may begin can be significantly higher or lower than that predicted by simple linear elastic analysis. The results show that, regardless of whether matrix cracking relieves or intensifies stress concentrations, a fair amount of cracking can occur locally at points of high stress within a component without destroying its integrity. The results emphasize the importance of inelastic straining in the direction of the fibers in redistributing stress.

(2) Double-Edge-Notched Specimens

A plate of a crossply brittle-matrix laminate with symmetric edge notches extending one quarter of the way across the section (notch length a) is loaded in tension, as shown in the inset of Fig. 5(A), and examined using the constitutive model for the same two composites that have been considered above. The loading is an applied displacement parallel to one set of fibers. This configuration closely replicates specimens for which experimental data has been obtained and which will be referenced below. The notch height is 3% of the specimen width and is very small compared to the height of the specimen. The notch tips are semicircular.

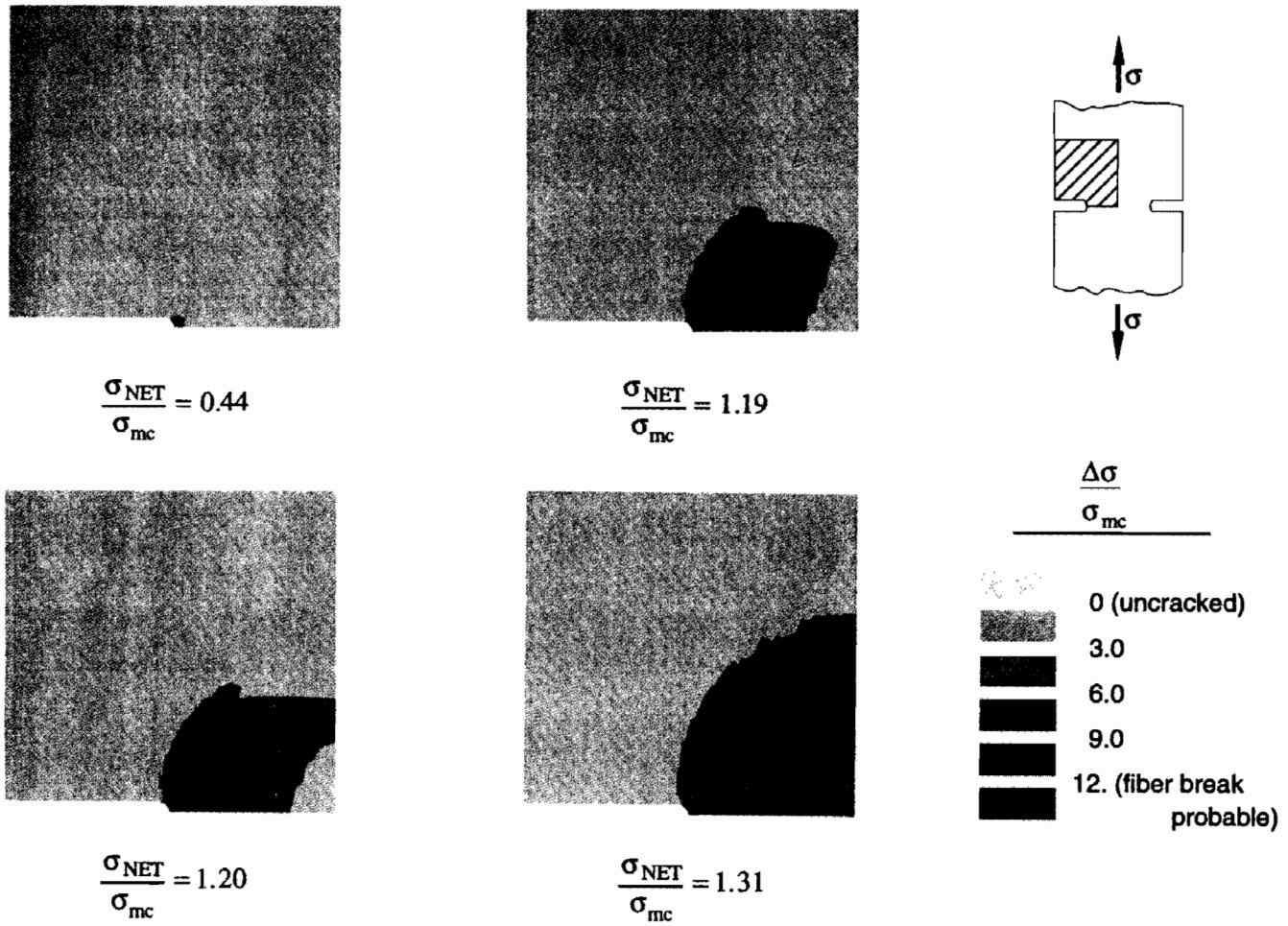

Fig. 6. Evolution of matrix cracking in a double-edge-notched SiC/CAS specimen loaded perpendicular to the notch plane. Outermost contour indicates the extent of the cracking region; inner contours indicate increased crack density. Extent of matrix cracking is described by the variable $\Delta\sigma$ (equal to $(1/\sigma_{mc})(\Delta\sigma_I^2 + \Delta\sigma_{II}^2)^{1/2}$), which is a normalized average of the stress deficits.

The boundary-value problems were again solved using the finite-element method. The solution procedure for the C/C specimen involved repeatedly stepping the applied displacement forward by a very small increment, iterating twice for the displacements within the domain, and proceeding to the next small displacement increment, regardless of whether equilibrium had been satisfied to within an acceptable tolerance. Convergence studies were conducted to ensure that the results presented here are independent of mesh size and displacement increment size. Convergence was attained with an analysis of 400 increments.

The solution for the SiC/CAS crossply was generated from the solution for a composite with a slightly stiffer 45° stress–strain curve. This solution served as the initial condition for each level of applied displacement.

Figures 5(A) and (B) show the engineering shear strain, γ_{xy}, normalized by the remote tensile strain, $\bar{\varepsilon}$, away from the notched area, along a line one-half crack length above the notches for the SiC/CAS and the C/C composites. In each of Figs. 5(A) and (B), the dashed line corresponds to the shear strains from a linear elastic analysis, and the solid lines correspond to computed normalized shear strains at the values of the net section stress, σ_{NET} (equal to $P/(2a)$), indicated for loads P ranging up to the load at which fiber breakage is predicted to occur. P is calculated as part of the solution to the boundary-value problem.

Figure 5(A) contains the numerical predictions for the C/C system. Normalized shear strains are plotted for loads in the linear range and for the load at which fiber fracture is predicted to begin. For the C/C composite, this occurs when the value of σ_{NET} is ~10% of the uniaxial matrix cracking stress, σ_{mc}. The shear-strain concentration is slightly reduced by matrix cracking but the straining remains almost proportional throughout the loading. This result is confirmed by experimental data reported by Evans,[8] which is superimposed onto Fig. 5(A). The Evans data, which is for several loads up to and beyond the stress at which fiber breaking is predicted to begin, fall within the range of shear strains that are observed in the analysis. This experimentally verifies that the strains remain almost proportional and that the model provides a highly accurate prediction of the strain field.

The numerical results and the experimental data for the C/C composite indicate that shear strains are concentrated in sharp shear bands extending vertically just behind the notch tips, as will be more evident in a plot shown later. Note that the peak value of γ_{xy} is greater than $\bar{\varepsilon}$ by a factor of >5 and is greater than the corresponding normalized strain level for the SiC/CAS composite in Fig. 5(B) by a factor of ~5. This large difference is due to the strong anisotropy of the C/C material.

Figure 5(B) reveals that the shear-strain concentrations in the SiC/CAS specimen in the elastic range are much smaller than those in the C/C specimen, which is expected because of the almost isotropic elastic properties of the SiC/CAS laminate. Matrix cracking that occurs around the notch tip eases the shear-strain concentrations very slightly by the time the first fiber fails, at a net section stress of ~130% of the uniaxial matrix cracking stress. Despite this relatively small redistribution, the strains again remain almost proportional.

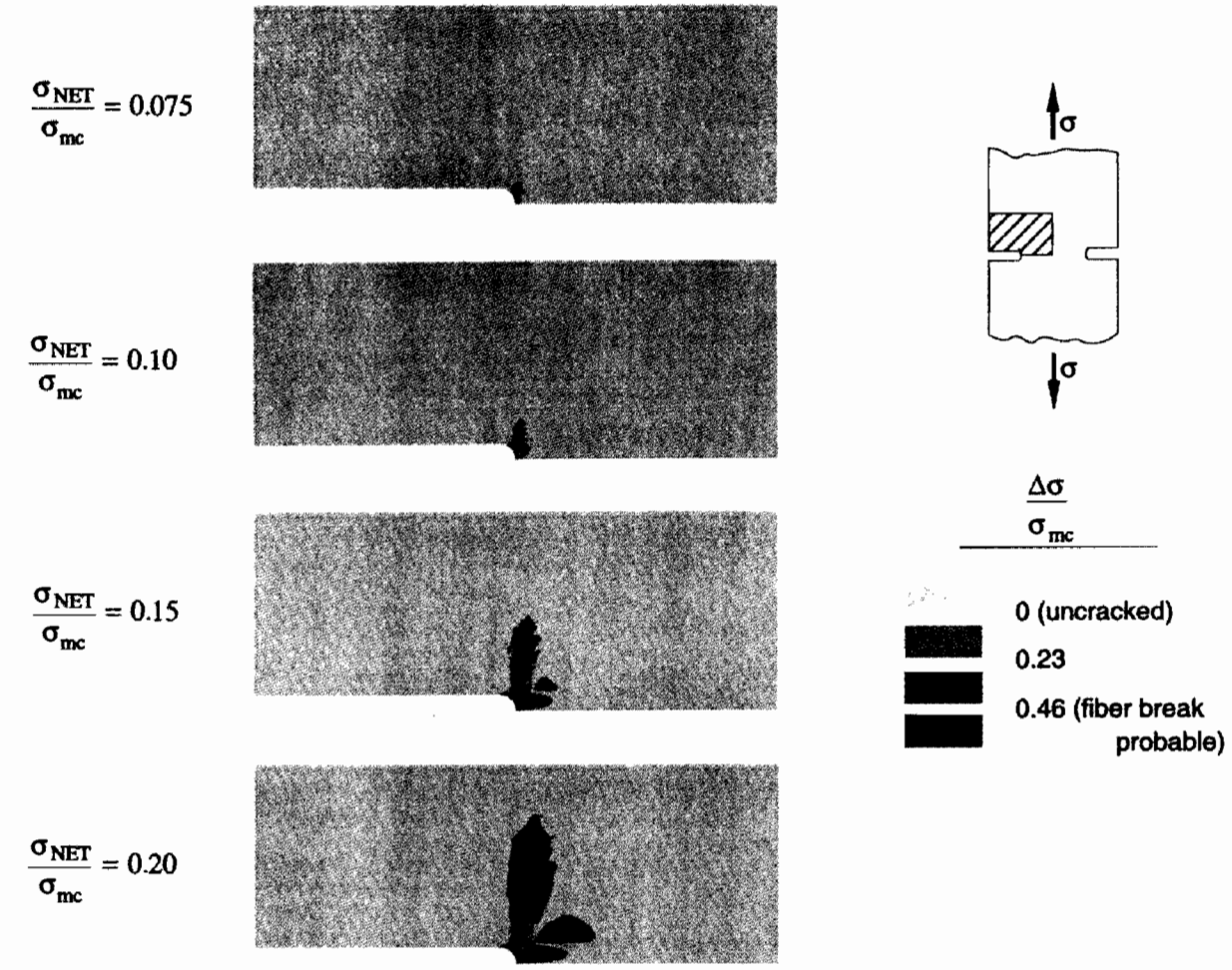

Fig. 7. Evolution of matrix cracking in a double-edge-notched C/C specimen loaded perpendicular to the notch plane. Outermost contour indicates the extent of the cracking region; inner contours indicate increased crack density. Extent of matrix cracking is described by the variable $\Delta\sigma$ (equal to $(1/\sigma_{mc})(\Delta\sigma_I^2 + \Delta\sigma_{II}^2)^{1/2}$), which is a normalized average of the stress deficits.

As in the case of a plate with a circular hole, cracking in the notched SiC/CAS specimen relieves stress concentrations, whereas cracking in the corresponding C/C specimen intensifies them. For the C/C specimen, the stress concentration, defined as the stress at the notch tip divided by the average stress across the ligament (σ_{NET}), is 10 for the elastic case, then increases to 14 at fiber failure. For the SiC/CAS specimen, the stress concentration decreases from the elastic value of 5.3 to ~2.5 at fiber failure.

The matrix cracking stress for an unnotched specimen of the C/C composite loaded parallel to one set of fibers is greater than that of the SiC/CAS composite by a factor of 4, and the stress at which fiber failure begins under such conditions is greater for the C/C composite by a factor of 1.25. However, because of the superior ability of the SiC/CAS composite to redistribute stresses through matrix cracking, the applied stress at which fiber failure is predicted to begin in the notched SiC/CAS specimen is higher than that predicted for the C/C composite. Stress redistribution due to matrix cracking more than doubles the load that is required to break fibers in the notched SiC/CAS specimen, relative to the load that is predicted based on the elastic stress concentration.

Figure 6 shows the development of matrix cracking in the SiC/CAS specimen. The contours are a normalized average of the principal stress deficits due to cracking: $\Delta\sigma \equiv (1/\sigma_{mc})(\Delta\sigma_I^2 + \Delta\sigma_{II}^2)^{1/2}$, where $\Delta\sigma_I$ and $\Delta\sigma_{II}$ are as defined in Eqs. (8*a*) and (8*b*), respectively. The outer contour, corresponding to where this quantity first becomes nonzero, depicts the extent of the region undergoing matrix cracking at a given load, and the inner contours indicate an increased crack density. The contour associated with the largest value of $\Delta\sigma$ shown indicates the stress decrease at which fiber failure would occur in a tensile test conducted at an angle of 45° to the fiber axes. Matrix cracks begin at the notch tips, then spread toward the center of the specimen. The first fiber failures are most likely to occur at the notch tips in the direction of the applied load.

Figure 7 shows the contours of maximum principal stress deficits that are predicted for the C/C composite. For this composite, cracking is initially concentrated in narrow shear bands above the notch tips, consistent with the behavior discussed earlier. A region of less-dense cracking develops along the ligament between the notches. For this specimen, fiber failure will most probably first occur on the notch boundaries, just behind the notch tips.

IV. Conclusions

Matrix cracking in brittle-matrix laminate composites can result in significant inelastic strain contributions, which, in turn, can lead to important stress redistribution at sites of high stress concentration. Matrix cracking can either ease or intensify stress concentrations. In this paper, a constitutive model has been presented that uses data from two uniaxial tests as input and is capable of predicting strains under proportional stressing for multiaxial plane-stress states. This model has been used to explore the effects of matrix cracking on stresses and strains in laminates containing holes and notches.

Acknowledgments: The authors are grateful to C. M. Cady, A. G. Evans, and F. E. Heredia for advice and assistance during the course of this research.

References

[1]C. M. Cady; unpublished work.
[2]D. Beyerle, S. M. Spearing, and A. G. Evans, "Damage Mechanisms and the Mechanical Properties of a Laminated 0/90 Ceramic Matrix Composite," *J. Am. Ceram. Soc.*, **75**, 3321–30 (1992).
[3]B. Harris, F. A. Habib, and R. G. Cooke, "Matrix Cracking and the Mechanical Behaviour of SiC/CAS Composites," *Proc. R. Soc. London, A*, **437**, 109–31 (1992).
[4]M.-Y. He and J. W. Hutchinson, "Kinking of a Crack Out of an Interface," *J. Appl. Mech.*, **57**, 270–78 (1990).
[5]P. H. Geubelle and W. G. Knauss, "Crack Propagation at and near Bimaterial Interfaces: Linear Analysis," *J. Appl. Mech.*, **61**, 560–66 (1994).
[6]K. R. Turner, J. S. Speck, and A. G. Evans, "Mechanisms of Deformation and Failure in Carbon-Matrix Composites Subject to Tensile and Shear Loading," *J. Am. Ceram. Soc.*, **78**, 1841–48 (1995).
[7]F. E. Heredia; unpublished work.
[8]A. G. Evans; private communication.
[9]C. M. Cady, T. J. Mackin, and A. G. Evans, "Silicon Carbide/Calcium Aluminosilicate: A Notch-Insensitive Ceramic-Matrix Composite," *J. Am. Ceram. Soc.*, **78**, 77–82 (1995).
[10]T. J. Mackin, K. E. Perry, J. S. Epstein, C. Cady, and A. G. Evans, "Strain Fields and Damage around Notches in Ceramic-Matrix Composites," *J. Am. Ceram. Soc.*, **79**, 65–73 (1996).
[11]C. M. Cady, K. E. Perry, and A. G. Evans, "Stress Redistribution around Mechanical Attachments in Ceramic-Matrix Composites," *Composites*, **26**, 683–90 (1995).
[12]A. G. Evans and F. W. Zok, "The Physics and Mechanics of Fibre-Reinforced Brittle Matrix Composites," *J. Mater. Sci.*, **29**, 3857–96 (1994).
[13]F. E. Heredia, S. M. Spearing, T. J. Mackin, M. Y. He, A. G. Evans, P. Mosher, and P. Brøndsted, "Notch Effects in Carbon Matrix Composites," *J. Am. Ceram. Soc.*, **77**, 2817–27 (1994).
[14]Z. C. Xia, R. R. Carr, and J. W. Hutchinson, "Transverse Cracking in Fiber-Reinforced Brittle Matrix, Cross-Ply Laminates," *Acta Metall. Mater.*, **41**, 2365–76 (1993).
[15]Z. C. Xia and J. W. Hutchinson, "Matrix Cracking of Cross-Ply Ceramic Composites," *Acta Metall. Mater.*, **42**, 1933–45 (1994).
[16]J. F. Wu, M. S. Shephard, G. J. Dvorak, and Y. A. Bahei-El-Din, "A Material Model for the Finite Element Analysis of Metal Matrix Composites," *Compos. Sci. Technol.*, **35**, 347–66 (1989).
[17]N. Laws, G. J. Dvorak, and M. Hejazi, "Stiffness Changes in Unidirectional Composites Caused by Crack Systems," *Mech. Mater.*, **2**, 123–37 (1983).
[18]G. J. Dvorak, "Transformation Field Analysis of Inelastic Composite Materials," *Proc. R. Soc. London, A*, **437**, 311–27 (1992).
[19]T. C. Kennedy and M. Wang, "Three Dimensional, Nonlinear Viscoelastic Analysis of Laminated Composites," *J. Compos. Mater.*, **28**, 902–24 (1994).
[20]G. J. Dvorak, Y. A. Bahei-El-Din, and A. M. Wafa, "Implementation of Transformation Field Analysis for Inelastic Composite Materials," *Comput. Mech.*, **14**, 201–28 (1994).
[21]X. Aubard, J. Lamon, and O. Allix, "Model of the Nonlinear Mechanical Behavior of 2D SiC–SiC Chemical Vapor Infiltration Composites," *J. Am. Ceram. Soc.*, **77**, 2118–26 (1994).
[22]F.-K. Chang and K.-Y. Chang, "A Progressive Damage Model for Laminated Composites," *J. Compos. Mater.*, **21**, 834–55 (1987).
[23]D. Krajcinovic, "Damage Mechanics," *Mech. Mater.*, **8**, 117–97 (1989).
[24]P. Ladeveze and E. Le Dantec, "Damage Modelling of the Elementary Ply for Laminated Composites," *Compos. Sci. Technol.*, **43**, 257–67 (1992).
[25]A. Matzenmiller and J. Sackman, "On Damage Induced Anisotropy for Fiber Composites," *Damage Mech.*, **3**, 71–96 (1994).
[26]D. R. Hayhurst, F. A. Leckie, and A. G. Evans, "Component Design-Based Model for Deformation and Rupture of Tough Fibre-Reinforced Ceramic Matrix Composites," *Proc. R. Soc. London, A*, **434**, 369–81 (1991).
[27]R. Talreja, "A Continuum Mechanics Characterization of Damage in Composite Materials," *Proc. R. Soc. London, A*, **399**, 195–216 (1985).
[28]R. Talreja, "Continnum Modeling of Damage in Ceramic Matrix Composites," *Mech. Mater.*, **12**, 165–80 (1991).
[29]D. H. Allen, C. E. Harris, and S. E. Groves, "A Thermomechanical Constitutive Theory for Elastic Composites with Distributed Damage—I. Theoretical Development," *Int. J. Solids Struct.*, **23**, 1301–18 (1987).
[30]P. H. Petit and M. E. Waddoups, "A Method of Predicting the Nonlinear Behavior of Laminated Composites," *J. Compos. Mater.*, **3**, 2–19 (1969).
[31]H. T. Hahn and S. W. Tsai, "Nonlinear Elastic Behavior of Unidirectional Composite Laminae," *J. Compos. Mater.*, **7**, 102–18 (1973).
[32]H. T. Hahn, "Nonlinear Behavior of Laminated Composites," *J. Compos. Mater.*, **7**, 257–71 (1973).
[33]Y. Surrel and A. Vautrin, "Plastic Behaviour of Fibrous Laminae," *Compos. Sci. Technol.*, **49**, 45–50 (1993).
[34]F.-K. Chang, R. A. Scott, and G. S. Springer, "Failure Strength of Nonlinearly Elastic Composite Laminates Containing a Pin Loaded Hole," *J. Compos. Mater.*, **18**, 465–77 (1984).
[35]S. M. Serabian and D. W. Oplinger, "An Experimental and Finite Element Investigation into the Mechanical Response of 0/90 Pin-Loaded Laminates," *J. Compos. Mater.*, **21**, 631–49 (1987).
[36]H. Ho, J. Morton, and G. L. Farley, "Non-Linear Numerical Analysis of the Iosipescu Specimen for Composite Materials," *Compos. Sci. Technol.*, **50**, 355–65 (1994).
[37]A. E. Green and W. Zerna, *Theoretical Elasticity*; pp. 350–51. Oxford University Press, London, U.K., 1968. □